ADVANCED MATERIALS
www.advmat.de

An Integrated 3D Hydrophilicity/Hydrophobicity Design for Artificial Sweating Skin (i-TRANS) Mimicking Human Body Perspiration

*Yucan Peng, Jiawei Zhou, Yufei Yang, Jian-Cheng Lai, Yusheng Ye, and Yi Cui**

Artificial skins reproducing properties of human skin are emerging and significant for study in various areas, such as robotics, medicine, and textiles. Perspiration, as one of the most imperative thermoregulation functions of human skin, is gaining increasing attention, but how to realize ideal artificial skin for perspiration simulation remains challenging. Here, an integrated 3D hydrophilicity/hydrophobicity design is proposed for artificial sweating skin (i-TRANS). Based on normal fibrous wicking materials, the selective surface modification with gradient of poly(dimethylsiloxane) (PDMS) creates hydrophilicity/hydrophobicity contrast in both lateral and vertical directions. With the additional help of bottom hydrophilic Nylon 6 nanofibers, the constructed i-TRANS is able to transport "sweat" directionally without trapping undesired excess water and attain uniform "secretion" of sweat droplets on the top surface, decently mimicking human skin perspiration situation. This fairly comparable simulation not only presents new insights for replicating skin properties, but also provides proper in vitro testing platforms for perspiration-relevant research, greatly avoiding unwanted interference from the "skin" layer. In addition, the facile, fast, and cost-effective fabrication approach and versatile usage of i-TRANS can further facilitate its application.

1. Introduction

Skin, the largest organ in humans and the first interface with the surrounding environment, plays significant roles in protection, sensation, insulation, and thermal regulation.[1] Aiming at reproducing specific properties or functions of skin, artificial skins, as well as skin-inspired devices, are emerging for assorted applications in recent years.[2,3] For instance, elastomeric materials such as silicone and polyurethanes are reported to simulate mechanical properties of human skin.[4–6] Metal-based composites/devices incorporating heating elements are utilized as skin simulants in terms of thermal properties.[7–9] Flexible and stretchable electronics that can sense touch are promising substitutes for tactile function of skin.[10–12] The advancement of artificial skins not only fosters the growth of robotics for which the skin component is indispensable for signal input and control, but also is meaningful for diverse fields, such as medicine, healthcare, and textiles, in which human skin alternatives are in extensive demand for testing.[13–15]

Perspiration is one of the most imperative thermoregulatory functions of human skin.[16,17] Sweat glands embedded in the skin across the body are responsible for secreting sweat.[18,19] The generated sweat is directly delivered to the slight hydrophobic skin surface[20] and form droplets (**Figure 1**a,b). To simulate the perspiration scenario on artificial skins is of great importance and gaining increasing attention. It is not only an indispensable component for artificial skin development, but also vital for in vitro tests for wearables, medicine, etc. The in vitro sweating skin that well replicates the perspiration condition of real one will facilitate research relevant to human body perspiration in various areas. However, how to realize ideal artificial skin for perspiration simulation remains challenging. For example, microfluidic devices made of layer(s) of membranes with laser cut pores usually require complicated fabrication, and uniform "sweat pore" activation still needs sufficiently high pressure provided.[21–24] For thermal assessment of textiles during perspiration, the water-fed porous metal plate covered by water-vapor permeable but liquid-water impermeable membrane can only simulate the vapor evaporation of human body, ignoring liquid sweat.[25,26] Supplying water through tiny tubes to holes at the manikin surface was performed, but the manufacturing of the system is very complex and costly.[27,28] The fabric skins (cotton, polyester, wool, etc.) acting as a wicking layer spread water out, whereas the "sweat" distribution situation and intrinsic severe water absorption by the fabrics cause this strategy inadequately reproduce human skin perspiration.[6,13]

Here, we propose an integrated 3D hydrophilicity/hydrophobicity design for artificial sweating skin (i-TRANS) to mimic

Y. Peng, J. Zhou, Y. Yang, Y. Ye, Y. Cui
Department of Materials Science and Engineering
Stanford University
Stanford, CA 94305, USA
E-mail: yicui@stanford.edu
J.-C. Lai
Department of Chemical Engineering
Stanford University
Stanford, CA 94305, USA
Y. Cui
Stanford Institute for Materials and Energy Sciences
SLAC National Accelerator Laboratory
2575 Sand Hill Road, Menlo Park, CA 94025, USA
The ORCID identification number(s) for the author(s) of this article can be found under https://doi.org/10.1002/adma.202204168.

DOI: 10.1002/adma.202204168

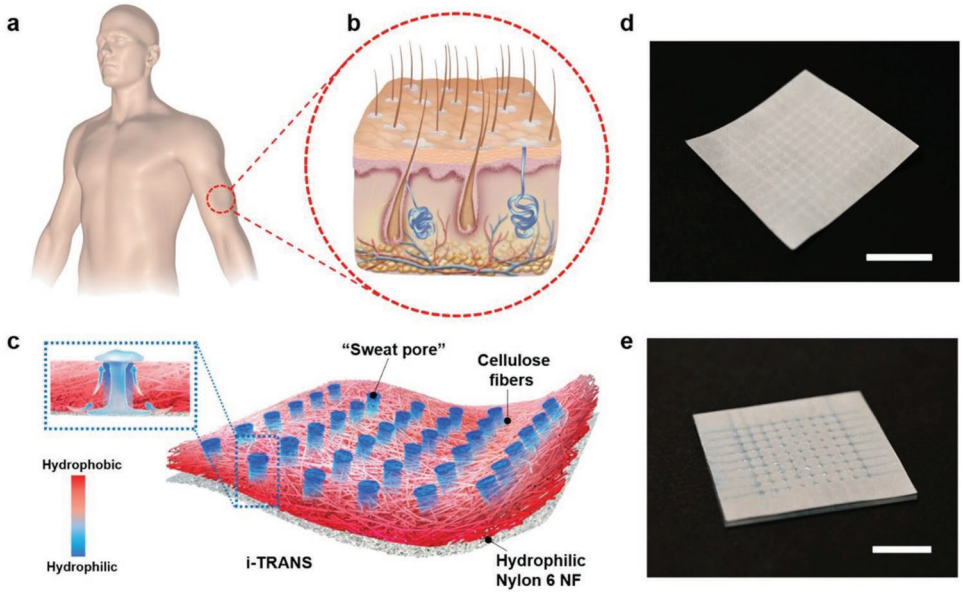

Figure 1. Concept illustration of integrated 3D hydrophilicity/hydrophobicity design for artificial sweating skin (i-TRANS) and its photographs. a) Schematic of human body. b) Schematic of human skin perspiration. c) Schematic of i-TRANS artificial sweating skin illustrating its structure and surface property. d) Photograph of i-TRANS in dry state. Scale bar: 1 cm. e) Photograph of i-TRANS in wet state mimicking human skin perspiration. Scale bar: 1 cm.

human body perspiration, highlighting 1) a facile, fast, and cost-effective fabrication method that applies to normal wicking materials, which is demonstrated to prepare the i-TRANS. 2) The i-TRANS properly simulates the human skin perspiration. It can efficiently transport water out directionally without trapping excess water and realize uniform "secretion" of sweat droplets on the top surface. The fairly comparable simulation of skin sweating can provide more reasonable measurements for tested materials, especially for thermal assessments, because less deviation will be caused by the inappropriate change of "skin" layer. 3) The i-TRANS is versatile for usage on different types of devices, including hot plate and manikin. The fabrication approach is highly flexible to produce i-TRANS in various areas and shapes, and based on substrates of different wicking materials.

2. i-TRANS Design and Fabrication

The i-TRANS is illustrated in Figure 1c. We selected common filter paper (Whatman No. 1) composed of cellulose microsized fibers as the substrate for demonstration. From a material perspective, paper materials offer advantageous properties that make them valuable materials in many application fields.[29] Cellulose filter papers show excellent mechanical flexibility, lightweight, biodegradability, and they are renewable.[30] Besides, the rich hydroxyl groups of cellulose benefit easy surface modification.[31] Cellulose filter papers and other paper materials have been widely used for microfluidic devices,[29] oil–water separation,[32–34] sensors,[35,36] actuators,[37] etc. In this work, the interconnected hydrophilic fiber network forming hierarchically porous structure renders it an ideal water wicking material, which is capable of efficiently transporting water via capillary effect. The scanning electron microscopy (SEM) images of the filter paper substrate without any modification are displayed in Figure S1 (Supporting Information). Selective surface modification was performed to change the surface property of the fibrous wicking substrate. The "sweat pores" (depicted in blue colors) are hydrophilic and retain water transportation ability, while the "non-pore" areas (depicted in red colors) are turned to be hydrophobic prohibiting superfluous water absorption. It is worthwhile to point out that the hydrophilicity gradient for "sweat pores" (increased hydrophilicity from bottom to top) is beneficial for one-way directional water transport from bottom to the top surface, due to the gradient wettability.[38–40] Besides, the fibrous wicking channels make every "sweat pore" easy to be activated for uniform sweating as long as water contacts the "sweat pore," not requiring high pressure or fast flow rate to overcome the Laplace pressure difference among pores, which is challenging for perforated dense membranes.[21,22] Moreover, we added a thin hydrophilic nanofiber (NF) layer at the very bottom underneath the microsized fibrous layer to spread water.[41] It further helps the entrance of water into the "sweat pores" and being transported out for formation of uniform sweating, especially advantageous for tiny amounts of water. Meanwhile, the NF layer does not cause obviously increased water absorption in the i-TRANS, due to its thin thickness (≈1 μm; Figure S2, Supporting Information) and low mass density (0.55 g m^{-2}). Figure 1d exhibits the photograph of an i-TRANS in dry sate, on which a 9 × 9 "sweat pore" array was fabricated. The photograph of wet i-TRANS for skin perspiration mimicking is shown in Figure 1e. It is clearly seen that a skin-like sweating condition, in which sweat droplets are uniformly distributed on the skin surface, can be realized by i-TRANS. It is worthwhile to mention that our i-TRANS design can be applied to different substrates of varied pore size, thickness,

and mass density. Here, we demonstrated the fabrication feasibility on other two filter papers (Whatman No. 4 and No. 5). The SEM images of blank Whatman No. 4 and No. 5 are exhibited in Figure S3 (Supporting Information), and the photographs of these wet i-TRANS-based substrates demonstrating skin perspiration simulation are shown in Figure S4 (Supporting Information).

The fabrication process of i-TRANS is illustrated in **Figure 2**a. Spray coating was utilized to modify the surface hydrophilicity/hydrophobicity of the normal wicking layer, where we adopted a fibrous cellulose filter paper (Whatman No. 1) as explained above. The base elastomer and curing agent of poly(dimethylsiloxane) (PDMS), which is testified to be a hydrophobic material,[42] were mixed and diluted by hexane for spray coating. A mask with covers for "sweat pores" was mounted on the filter paper. The masked side would be used as the bottom side, while the other side is the top side, for sweat mimicking. We divided the sample surface into four areas and denoted as "bottom side's non-pore area" ("Bottom_Non-pore"), "top side's non-pore area" ("Top_Non-pore"), "bottom side's pore area" ("Bottom_Pore"), and "top side's pore area" ("Top_Pore"), respectively. Bottom_Non-pore was modified to be hydrophobic due to the addition of PDMS. Also, Top_Non-pore became hydrophobic as well owing to the capillary transport of PDMS solution from the bottom side. Nevertheless, Top_Non-pore is less hydrophobic than Bottom_Non-pore due to the diffusion gradient. As for Bottom_Pore and Top_Pore, which were covered by the mask during spray coating, PDMS solution inevitably diffused laterally into these areas before the total evaporation of hexane. However, the wicking capability of

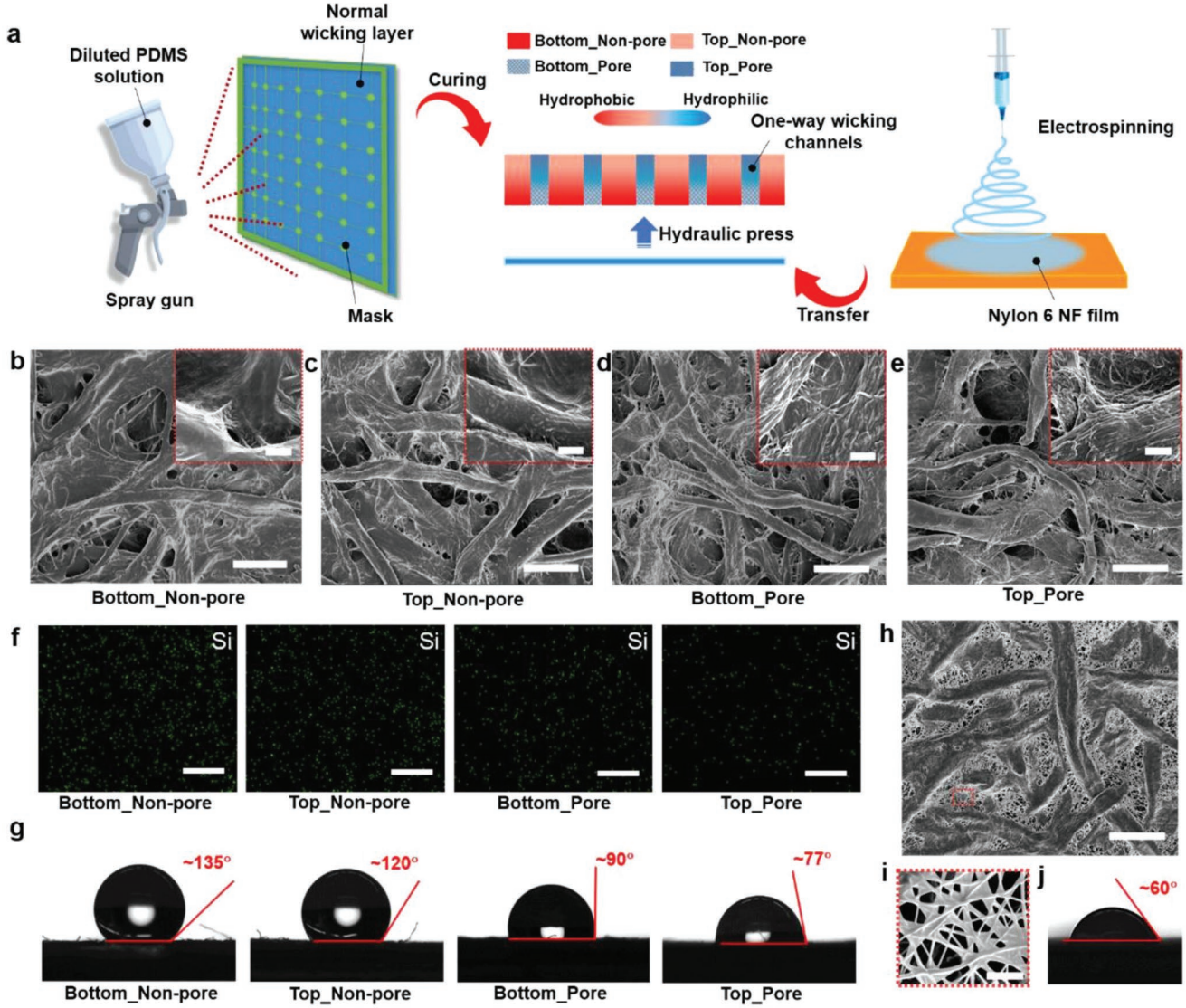

Figure 2. Fabrication of i-TRANS and its surface property characterization. a) Schematic of fabrication process of i-TRANS. b–e) SEM images of different areas on i-TRANS without Nylon 6 NF film. Scale bars: 50 µm. The insets are magnified SEM images. Scale bars: 5 µm. f) EDS mapping of Si element in different areas on i-TRANS without Nylon 6 NF film. Scale bars: 10 µm. g) Water contact angles measured on different areas on i-TRANS without Nylon 6 NF film. h) SEM image of bottom side of i-TRANS (with the addition of Nylon 6 NFs). Scale bar: 50 µm. i) Magnified SEM image showing the Nylon 6 NF network. Scale bar: 3 µm. j) Water contact angle of Bottom_Non-pore covered with Nylon 6 NFs.

hydrophilic cellulose fibrous network was maintained. Notably, Top_Pore retains to be more hydrophilic than Bottom_Pore because such an area obtained the least PDMS solution diffusion. It results in the hydrophilicity gradient and endows i-TRANS with directional water transport ability from bottom to top. It is very important to optimize the amount of coated PDMS to achieve the desired i-TRANS design. For Whatman No. 1 of 25 cm^2, a PDMS loading mass of ≈0.032 g is optimal, which is identified experimentally. If the PDMS loading mass reaches ≈0.05 g, the "sweat pores" would be blocked partially. When the PDMS loading mass is ≈0.1 g, water cannot be transported through the "sweat pores" due to the excessive PDMS (Figure S5a, Supporting Information). On the other hand, the PDMS loading mass should not be too low, or the PDMS coating cannot prevent water sufficiently for the non-pore area. As shown in Figure S5b (Supporting Information), the prepared sample with 0.0095 g PDMS absorbs water other than the "sweat pores," which is not ideal for the i-TRANS design. Besides, we identified the optimized PDMS mass loadings for Whatman No. 4 and No. 5 (25 cm^2) are 0.035 and 0.09 g, respectively. The dimension of covered parts on the mask plays an important role in controlling the "sweat pore" size and realizing the directional water transport ability. Too small covered area cannot prevent PDMS diffusion sufficiently to preserve water transportation channels. Also, too large covered area is not able to construct the hydrophilicity difference between Bottom_Pore and Top_Pore for the directional water transport. The size of covered area should be optimized wisely according to the desired "sweat pore" size, PDMS solution concentration, and substrate wicking property. Lastly, the thin hydrophilic Nylon 6 NF film prepared via electrospinning was transferred onto the bottom side and fixed by hydraulic press.

3. 3D Hydrophobicity/Hydrophilicity Contrast Characterization

Figure S1 (Supporting Information) exhibits the SEM images of normal wicking layer without any surface modification. Fibers in different sizes of diameter (tens of micrometers to sub-micrometers), hierarchical pores, and rough surface morphology of relatively big fibers can all be distinctly identified. The SEM images of normal wicking layer modified by excessive PDMS via dip coating in the diluted PDMS solution are displayed in Figure S6 (Supporting Information). It is clear seen that PDMS blocks the pores and turns the fiber surface to be relatively smooth with polymer wrinkles. Figure 2b–e displays the SEM images (insets show the ones with larger magnification) of the four areas in i-TRANS before Nylon 6 NF film was applied. Through comparing with Figures S1 and S6 (Supporting Information), it can be recognized that PDMS covers the fiber surfaces in Bottom_Non-pore (Figure 2b) turning the surface morphology to be smoother and fills in the some of the small pores. Similar morphology change because of PDMS modification can be witnessed for Top_Non-pore, but it indicates that less PDMS was attached to the fiber surface considering that rougher fiber surface and more pores can be seen (Figure 2c). On the other hand, no apparent morphology alteration was perceived for Bottom_Pore (Figure 2d) and Top_Pore (Figure 2e). Furthermore, energy dispersive spectroscopy (EDS) was used to map the silicon (Si) element distribution in the four areas. As shown in Figure 2f, an obvious descending trend of Si counts demonstrates the decreased amounts of PDMS applied to Bottom_Non-pore, Top_Non-pore, Bottom_Pore, and Top_Pore (see Figure S7 in the Supporting Information for the EDS spectra). The surface modification variation leads to the hydrophilicity/hydrophobicity gradients across the vertical direction for both "sweat pores" and "non-pore" parts. We measured water contact angles for these four areas, and representative photographs are displayed in Figure 2g. The Bottom_Non-pore and Top_Non-pore reveal evident hydrophobicity with water contact angles of ≈135° and ≈120°, respectively. Differently, the water contact angles measured within the time zone of stably standing droplet on Bottom_Pore and Top_Pore are ≈90° and ≈77°, respectively. The statistical measured water contact angles at five randomly selected locations (ten data points) for each area are shown in Figure S8 (Supporting Information). The discrepancy in water contact angle validates the hydrophilicity/hydrophobicity difference created by the PDMS spray coating. Even though these areas do not show very strong hydrophilicity, the capillary effect resulted from the porous structure constructed by the fibers works for water wetting. Besides, the hydrophilicity gradient of "sweat pores" across the vertical direction guarantees the one-way directional water transport. As shown in Movie S1 and Figure S9a (Supporting Information), the water droplet (slightly larger than the "pore") loaded onto the Bottom_Pore can be transported fast through the sample, and water droplet accumulates on the other side. As a comparison, the same volume of water droplet loaded onto the Top_Pore hardly penetrates across the sample (Movie S2 and Figure S9b, Supporting Information). Figure 2h exhibits the SEM image of bottom side of i-TRANS with the addition of Nylon 6 NF film. The Nylon 6 NFs are pressed into the pores among cellulose fibers as well as the cellulose fiber skeletons, forming an interconnected hydrophilic NF network (Figure 2h,i). The SEM image showing the cross section of i-TRANS is displayed in Figure S10 (Supporting Information). The water contact angle of Nylon 6 NF covered Bottom_Non-pore is ≈60° (Figure 2j), indicating that the i-TRANS bottom achieves decent hydrophilicity for spreading water with the help of Nylon 6 NF film. The statistical measured water contact angle data are shown in Figure S8 (Supporting Information) as well. This water contact angle is slightly lower than the reported water contact angle values for Nylon 6 in literature (≈70°–80°), which is perhaps due to the porous structure of the nanofiber mat.

4. i-TRANS Performance Evaluation for Sweating Mimicking

We characterized how the i-TRANS performs in working condition, which means how i-TRANS handles water for skin perspiration simulation. First, the conditions of i-TRANS for given amounts of supplied water (0.05, 0.1, 0.2, and 0.5 mL for a 5 cm × 5 cm sample) were characterized, as shown in **Figure 3**a. For comparison, the sample conditions of a normal wicking layer (blank filter paper) and a perforated hydrophilic membrane

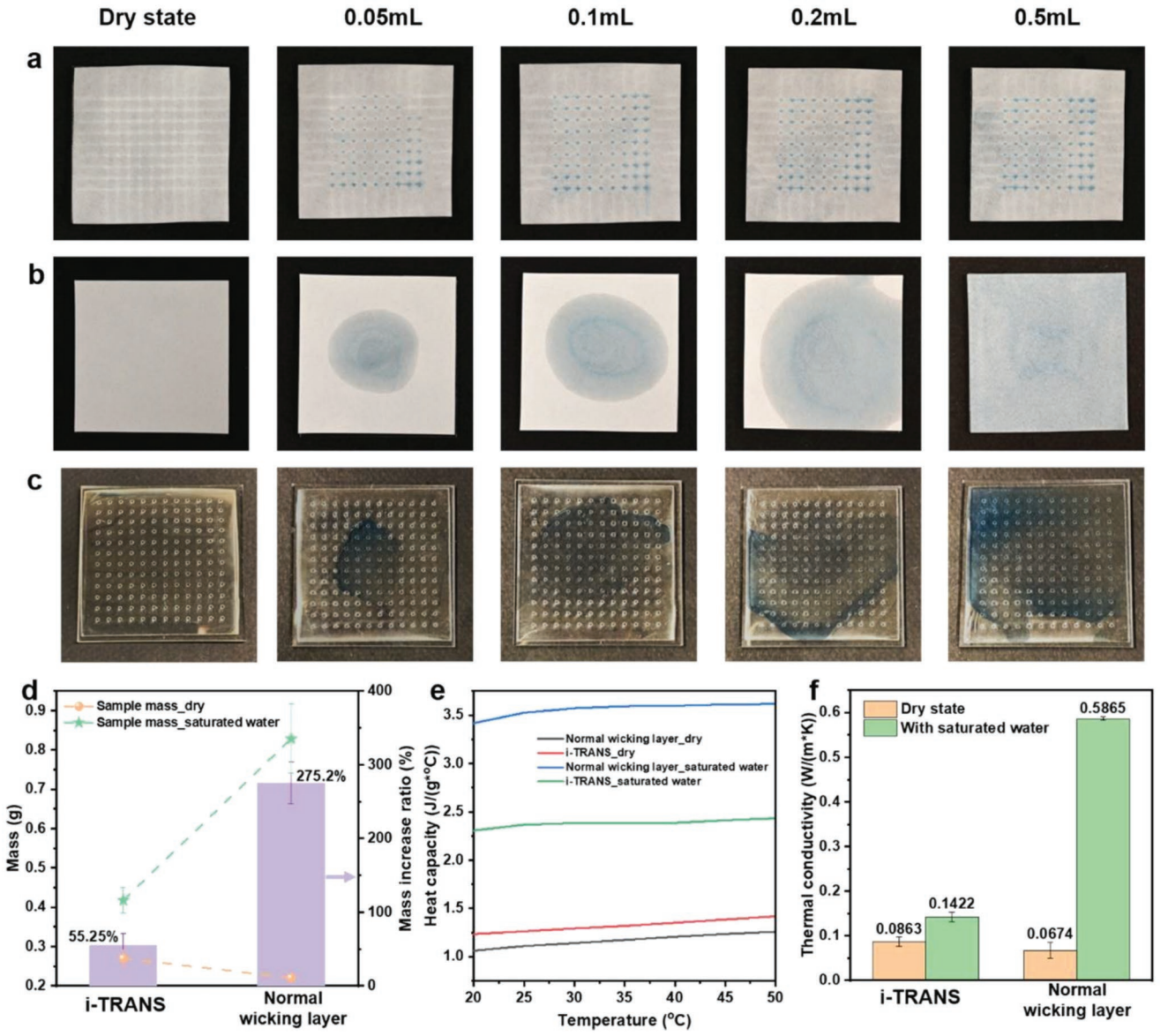

Figure 3. Performance evaluation under sweating mimicking condition. a–c) Photographs of i-TRANS (a), a normal wicking layer (b), and a perforated PET membrane (c) when different amounts of water were supplied underneath them. d) Sample mass of i-TRANS and normal wicking layer in dry state and with saturated water, and the mass increase ratio. e) Measured heat capacity of i-TRANS and normal wicking layer in dry state and with saturated water in the temperature range of 20–50 °C. f) Measured thermal conductivity of i-TRANS and normal wicking layer in dry state and with saturated water.

(polyester membrane with holes) with the same amounts of supplied water are shown in Figure 3b,c, respectively. Blue dye was added to water for convenient observation. For the normal wicking layer, its strong wicking capability enables it to absorb water and spread it out into elliptical shapes within a certain area. With a large volume of water, the wicking layer became totally wet. However, this is not how real skin performs when sweat is generated. Different from wicking materials, the perforated hydrophilic polyester (PET) membrane does not absorb water at all. When placed on a certain amount of water, water distribution is in a more limited region and uniform "sweating" cannot be realized. Even with compatible water reservoir underneath and pressure supply devices, the uniform "sweat pore" activation is arduous. In contrast, even a tiny amount of water (0.05 mL) is sufficient to occupy nearly all the "sweat pores" on our i-TRANS and be transported onto the outer surface forming uniform "sweat" droplets, which results from the water prohibition by hydrophobic non-pore areas and restricted water absorption and transportation by only the "sweat pores." Larger volumes of water realize uniform "sweating" more easily.

Besides, it is noteworthy to highlight the great reduction of water absorption capacity of i-TRANS, compared to the normal wicking layer. In addition to the intuitive demonstration in Figure 3a,b, we measured the water absorption capacity of i-TRANS and normal wicking layer by weighing the sample mass in the dry state and with saturated water. As shown in Figure 3d, the mass increase ratio of normal wicking layer with saturated water is 275.2%, while that of our i-TRANS is only

55.25%. It means i-TRANS reduces the amount of absorbed water to be less than 1/5 of the unmodified normal wicking layer. The high water absorption capacity of a normal wicking layer indicates that the "skin" layer first absorbs water substantially before delivering "sweat" to the skin outer surface and the materials on it for testing, in significant contrast to the actual perspiration situation in human body. The critical water absorption also causes significant change of physical properties of the "skin" itself, such as heat capacity and thermal conductivity. Conversely, the suppressed water absorption in i-TRANS can effectively alleviate this problem. Figure 3e exhibits the measured heat capacity of i-TRANS and normal wicking layer in dry and saturated water states. Taking 35 °C as an example, heat capacity of normal wicking layer increases from 1.174 J (g °C) $^{-1}$ (dry) to 3.592 J (g °C) $^{-1}$ (saturated water), whereas heat capacity of our i-TRANS only increases from 1.319 J (g °C) $^{-1}$ (dry) to 2.382 J (g °C) $^{-1}$ (saturated water). Similarly, the increase of thermal conductivity from dry to saturated water state for i-TRANS is much smaller than the normal wicking layer (Figure 3f).

5. Demonstration in a Textile Testing Scenario

Furthermore, we compared the measurements for an identical piece of cotton fabric by using i-TRANS and the normal wicking layer for "skin perspiration" on an artificial skin testing device. As illustrated in **Figure 4**a, a heater placed on an insulating foam was used to simulate the heat generation of human body. Thermocouples and a water inlet, which were sealed in a thin acrylic board, were attached to the heater. Then, the i-TRANS or normal wicking layer was added as the top layer for the whole artificial skin device, serving as the "sweating skin". Water heated to 37 °C was pumped in at a specific rate continuously supplying "sweat" to the bottom side of i-TRANS or normal wicking layer. The cotton fabric for testing sat on the top of the artificial skin device. First, the water pumping rate (sweating rate) was set as 0.8 mL h^{-1} for the 25 cm^2 testing area (i.e., 320 mL (h m^2) $^{-1}$), which can be considered as a moderate sweating rate for human body. A constant power density of 456 W m^{-2} was applied. We measured the mass increase of i-TRANS/normal wicking layer as well as the cotton fabric at intervals and the thermocouple recorded the "skin" temperature.

Exceptionally different behaviors were observed for i-TRANS and normal wicking layer due to their different working mechanism. The normal wicking layer can spread water out but it held water within its own fibrous network due to its strong water absorption capability. As a result, the normal wicking layer as "skin" trapped an undesirably large amount of water in itself. As shown in the blue curves in Figure 4b, the normal wicking layer skin held much more water than the cotton fabric during

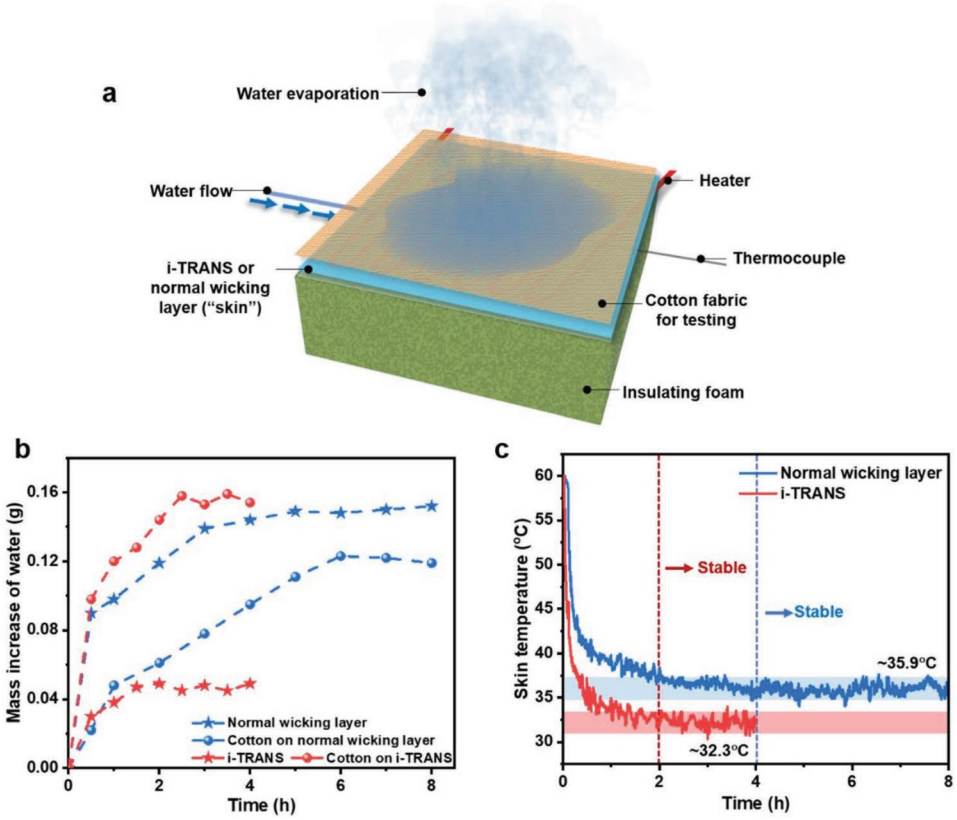

Figure 4. Demonstration in a textile testing scenario. a) Schematic of artificial skin testing device for comparison between i-TRANS and normal wicking layer as the "skin." b) Measured mass increase of water for i-TRANS, normal wicking layer, and the tested cotton fabric on them. c) Measured skin temperature during the tests with i-TRANS or normal wicking layer.

the 8 h measurement period, and water in "skin" was around twice amount as that in the cotton fabric at the beginning. This is very unsimilar to the real scenario of human body skin that transports sweat instead of absorbing sweat. In contrast, in such a test, the i-TRANS was more likely to serve as a transfer media to efficiently deliver "sweat," mimicking the working mechanism of human skin. Thus, water mass increase mainly happened in the cotton fabric rather than in the i-TRANS (red curves in Figure 4b). Photographs of normal wicking layer and i-TRANS during the measurement are displayed in Figures S11 and S12 (Supporting Information), respectively. The difference in "sweating" behavior also resulted in the difference in stabilization time. For the normal wicking layer, due to the water absorption competition between the "skin" and tested fabric, and evaporation and condensation processes, much longer time was needed for testing stabilization. Nevertheless, it took much shorter time for our i-TRANS. This information can be derived either from the water mass increase curves in Figure 4b or the recorded skin temperature data (Figure 4c), revealing that i-TRANS shortened the stabilization time to be around half of that with normal wicking layer. In addition, the stable temperature with i-TRANS was prominently lower than that with the normal wicking layer. This is because evaporation at equilibrium mostly occurred at the cotton fabric surface in the case of i-TRANS. Conversely, in the case of normal wicking layer, a great portion of evaporation occurred on the "skin" and condensation also happened between "skin" and the fabric, releasing heat and increasing skin temperature. This is another indicator that i-TRANS can reduce disturbance for moisture management testing of fabrics. We also performed the measurements at a higher "sweating" rate (520 mL (h m^2) $^{-1}$). Either i-TRANS or normal wicking layer required much longer time to reach equilibrium, but similar trends of sample mass increase and skin temperature were detected (Figures S13 and S14, Supporting Information).

6. Conclusion

We have reported a new integrated 3D hydrophilicity/hydrophobicity design for artificial skin simulating human skin perspiration, and demonstrated a facile and cost-effective fabrication method. The design of selective surface modification on normal fibrous wicking materials to create hydrophilicity/hydrophobicity contrast and gradient in both the lateral and vertical directions renders our i-TRANS capable of directionally transporting "sweat" efficiently and uniformly. In thermal assessments relevant to perspiration, these features make i-TRANS a promising sweating skin simulant, well mimicking skin perspiration, and not imposing unwanted interference for tested materials. We believe that this work provides new insights for simulation of skin sweating, and can be readily applied in various testing scenarios and accelerates the development of relevant industries. For the further advancement of i-TRANS, the fabrication process can be extended to elastic/stretchable substrates capable of wicking, which can be even more versatile to adapt to testing devices in various shapes more conformally. Also, the i-TRANS design and structure can be further optimized to better replicate skin properties (roughness, sweat pore size, sweat pore density, etc.). Besides, the i-TRANS design for perspiration mimicking can be incorporated with other artificial skins with specific features (e.g., mechanical properties, thermal properties, and tactile functions) to develop next-generation artificial skins with comprehensive properties well reproducing human skin.

7. Experimental Section

Fabrication of i-TRANS: The cellulose filter paper (Qualitative, Whatman) was selected as the normal wicking layer. A CO_2 laser cutter (Epilog Fusion M2) was used to cut an acrylic board into the mask. The mask was mounted on the top of the filter paper. PDMS base and curing agent (Sylgard 184, Dow Corning) (mass ratio was 10:1) were dispersed into hexane (Fisher Scientific) with a volume ratio of 1:2.5. A spray gun (3 M) was used to spray the PDMS solution onto the masked filter paper. The distance between filter paper and spray head was about 20 cm. The volume of PDMS solution added into the spray gun head was around 1 mL for a 5 cm × 5 cm sample. Then, the sample was placed in a 70 °C oven for drying and curing. Nylon 6 NF film was made by the electrospinning method, which was used in the previous work.[32] The prepared Nylon 6 NF film was cleaned by an air plasma decontaminator (Evactron, XEI Scientific) for 5 min and transferred to laminate on the bottom side (side directly facing PDMS spray coating) of the PDMS-modified filter paper. A hydraulic press (MTI) was used to press Nylon 6 NFs onto the filter paper.

Material Characterization: The SEM images were taken by FEI Nova NanoSEM 450 (5 kV). The EDS characterization was done using an FEI Magellan 400 XHR SEM equipped with Thermo Fisher Scientific Pathfinder EDS UltraDry 60 M. The water contact angle was measured by a contact angle goniometer (Rame-Hart 290), with a water droplet volume of 1 µL. The water droplet was small enough to only contact the interested area, not affected by the surrounding areas of different types. The heat capacity measurement was done using a differential scanning calorimeter (TA instrument Q2500).

Thermal Conductivity Measurement: The thermal conductivity was measured by the heat flowmeter method. The measured sample was placed in between two aluminum (Al) plates, whose temperatures were controlled to be 18 and 33 °C using thermoelectric modules separately. Two thermocouples (K type, Omega Engineering) were embedded in the Al plate, near the surface. A heat flux sensor (FHF03, Hukseflux) with an effective sensing area of 2.5 cm^2 was mounted within the bottom Al plate. A proportional–integral–derivative (PID) control algorithm was utilized to stabilize the temperatures of the Al plates at the set points (within 0.05 °C) and the data were obtained only after the temperatures were stabilized. The thermal conductivity was calculated by $k = (VSt)/\Delta T$, where V is the voltage output of the heat flux sensor, S is its sensitivity (W m^{-2} V^{-1}), t is the thickness of measured material, and ΔT is the temperature difference between two Al plates. In these measurements, two copper (Cu) plates (≈335 µm thick) were used to sandwich the sample(s), and they were sealed tightly in a polyethylene (PE) bag (≈50 µm thick) for water evaporation prohibition. For dry samples, only the two Cu plates with the PE bag were measured first as the reference. Then one piece of dry sample was inserted between the Cu plates and data were measured. Thermal resistance data can be converted by thermal conductivity and thickness, and thermal resistance of only the dry sample can be calculated by thermal resistance difference between "sample + reference" and reference. Next, thermal conductivity of the dry sample can be derived by the thermal resistance and its thickness. For the thermal conductivity measurements for wet samples, thermal conductivity of one piece of the wet sample inserted between the Cu plates together with the PE bag first was measured. Then, two or multiple pieces of wet samples were measured with the same Cu plates and PE bag. The thermal conductivity of wet sample can be derived in a similar way as for the dry sample. The thermal conductivity obtained this way included the interfacial resistance, which could not be separated in this measurement.

Artificial Skin Test: A polyimide-insulated flexible heater (McMaster-Carr, 25 cm^2) was used, which was connected to a power supply (Keithley 2400) to generate heat. The heater was placed on a foam (10 cm thick) for heat insulation. An acrylic board (1.5 mm thick) with two grooves made by laser cutting (Epilog Fusion M2) was fixed on the top surface of the heater. A thermocouple (≈0.1 mm in diameter, K-type, Omega) was sealed in one groove for skin temperature measurement, and a needle for delivering water that was connected to a tube and a syringe pump (Harvard, PHD 2000) was sealed in the other groove. The i-TRANS or a normal wicking layer was placed on the top of the acrylic board. The cotton fabric (single jersey knit, 135 g m^{-2}, ≈400 µm thickness, Dockers) for testing was put on the very top. During the measurements, pumped water in the tube was heated to be 37 °C by a PID temperature controller (Omega Engineering) before flowing onto the artificial skin. The mass of i-TRANS or normal wicking layer as well as the cotton fabric was measured by a balance (U. S. Solid, 0.001 g accuracy). All the tests were performed in an environment of 20 ± 0.3 °C and 35 ± 5% relative humidity.

Supporting Information

Supporting Information is available from the Wiley Online Library or from the author.

Acknowledgements

Part of this work was performed at the Stanford Nano Shared Facilities and the Stanford Nanofabrication Facility.

Conflict of Interest

The authors declare no conflict of interest.

Data Availability Statement

The data that support the findings of this study are available from the corresponding author upon reasonable request.

Keywords

artificial skin, perspiration mimicking, surface hydrophilicity/hydrophobicity, surface modification, textiles

Received: May 9, 2022
Revised: August 2, 2022
Published online: October 3, 2022

[1] N. G. Jablonski, *Skin: A Natural History*, University of California Press, Los Angeles, CA, USA **2013**.
[2] M. Wang, Y. Luo, T. Wang, C. Wan, L. Pan, S. Pan, K. He, A. Neo, X. Chen, *Adv. Mater.* **2021**, *33*, 2003014.
[3] M. Amjadi, K. U. Kyung, I. Park, M. Sitti, *Adv. Funct. Mater.* **2016**, *26*, 1678.
[4] R. Shimizu, Y. Nonomura, *J. Oleo Sci.* **2018**, *67*, 47.
[5] J. Jachowicz, R. Mcmullen, D. Prettypaul, *Skin Res. Technol.* **2007**, *13*, 299.
[6] A. K. Dąbrowska, G.-M. Rotaru, S. Derler, F. Spano, M. Camenzind, S. Annaheim, R. Stämpfli, M. Schmid, R. M. Rossi, *Skin Res. Technol.* **2016**, *22*, 3.
[7] P.-C. Hsu, A. Y. Song, P. B. Catrysse, C. Liu, Y. Peng, J. Xie, S. Fan, Y. Cui, *Science* **2016**, *353*, 1019.
[8] Y. Peng, J. Chen, A. Y. Song, P. B. Catrysse, P. C. Hsu, L. Cai, B. Liu, Y. Zhu, G. Zhou, D. S. Wu, H. R. Lee, S. Fan, Y. Cui, *Nat. Sustainability* **2018**, *1*, 105.
[9] L. Cai, Y. Peng, J. Xu, C. Zhou, C. Zhou, P. Wu, D. Lin, S. Fan, Y. Cui, *Joule* **2019**, *3*, 1478.
[10] J. A. Rogers, T. Someya, Y. Huang, *Science* **2010**, *327*, 1603.
[11] S. Wang, J. Xu, W. Wang, G. J. N. Wang, R. Rastak, F. Molina-Lopez, J. W. Chung, S. Niu, V. R. Feig, J. Lopez, T. Lei, S. K. Kwon, Y. Kim, A. M. Foudeh, A. Ehrlich, A. Gasperini, Y. Yun, B. Murmann, J. B. H. Tok, Z. Bao, *Nature* **2018**, *555*, 83.
[12] I. You, D. G. MacKanic, N. Matsuhisa, J. Kang, J. Kwon, L. Beker, J. Mun, W. Suh, T. Y. Kim, J. B. H. Tok, Z. Bao, U. Jeong, *Science* **2020**, *370*, 961.
[13] B. Koelblen, A. Psikuta, A. Bogdan, S. Annaheim, R. M. Rossi, *Int. J. Biometeorol.* **2017**, *61*, 1519.
[14] R. Neupane, S. H. S. Boddu, J. Renukuntla, R. J. Babu, A. K. Tiwari, *Pharmaceutics* **2020**, *12*, 152.
[15] C. Wang, D. Hwang, Z. Yu, K. Takei, J. Park, T. Chen, B. Ma, A. Javey, *Nat. Mater.* **2013**, *12*, 899.
[16] J. D. Hardy, *Proc. Natl. Acad. Sci. USA* **1937**, *23*, 631.
[17] E. R. Nadel, R. W. Bullard, J. A. Stolwijk, *J. Appl. Physiol.* **1971**, *31*, 80.
[18] K. Sato, W. H. Kang, K. Saga, K. T. Sato, *J. Am. Acad. Dermatol.* **1989**, *20*, 537.
[19] G. W. Mack, E. R. Nadel, in *Handbook of Physiology, Sect 4: Environmental Physiology* (Eds: M. J. Fregly, C. M. Blatteis), Oxford University Press, New York **1996**, pp. 187–214.
[20] Z. Sonner, E. Wilder, J. Heikenfeld, G. Kasting, F. Beyette, D. Swaile, F. Sherman, J. Joyce, J. Hagen, R. Naik, *Biomicrofluidics* **2015**, *9*, 031301.
[21] L. Hou, J. Hagen, X. Wang, I. Papautsky, R. Naik, N. Kelley-Loughnane, J. Heikenfeld, *Lab Chip* **2013**, *13*, 1868.
[22] A. Koh, D. Kang, Y. Xue, S. Lee, R. M. Pielak, J. Kim, T. Hwang, S. Min, A. Banks, P. Bastien, M. C. Manco, L. Wang, K. R. Ammann, K. Jang, P. Won, S. Han, R. Ghaffari, U. Paik, M. J. Slepian, G. Balooch, Y. Huang, J. A. Rogers, *Sci. Transl. Med.* **2016**, *8*, 366ra165.
[23] D. Hansen, S. Z. Moghaddam, J. Eiler, E. Thormann, *ACS Appl. Polym. Mater.* **2020**, *2*, 1535.
[24] G. Rabost-Garcia, J. Farré-Lladós, J. Casals-Terré, *Membranes* **2021**, *11*, 150.
[25] ASTM Standard F2370-10, *Standard Test Method for Measuring the Evaporative Resistance of Clothing Using a Sweating Manikin*, ASTM International, West Conshohoken, PA, USA **2005**.
[26] International Standard ISO11092, *Textiles - Physiological effects - Measurement of thermal and water vapor resistance under steady-state conditions (sweating guarded hotplate test)*, Published by ISO copyright office, **2014**.
[27] Z.-R. Li, W.-C. Jiang, L.-J. Wang, W.-D. Meng, F.-L. Qing, *Text. Res. J.* **2007**, *77*, 227.
[28] M. Guan, S. Annaheim, M. Camenzind, J. Li, S. Mandal, A. Psikuta, R. M. Rossi, *Text. Res. J.* **2019**, *89*, 4537.
[29] A. Böhm, M. Biesalski, *MRS Bull.* **2017**, *42*, 356.
[30] Ç. Koşak Söz, S. Trosien, M. Biesalski, *ACS Appl. Mater. Interfaces* **2018**, *10*, 37478.
[31] A. W. Martinez, S. T. Phillips, G. M. Whitesides, *Anal. Chem.* **2010**, *82*, 3.
[32] S. Wang, K. Liu, X. Yao, L. Jiang, *Chem. Rev.* **2015**, *115*, 8230.
[33] Z. Yin, F. Yuan, M. Li, M. Xue, D. Zhou, Y. Chen, X. Liu, Y. Luo, Z. Hong, C. Xie, J. Ou, *Prog. Org. Coat.* **2021**, *157*, 106311.
[34] M. Zhang, C. Wang, S. Wang, Y. Shi, J. Li, *Appl. Surf. Sci.* **2012**, *261*, 764.
[35] Q. Wang, Y. Liu, Y. Bai, S. Yao, Z. Wei, M. Zhang, L. Wang, L. Wang, *Anal. Chim. Acta* **2019**, *1049*, 170.

[36] Q. Li, H. Liu, S. Zhang, D. Zhang, X. Liu, Y. He, L. Mi, J. Zhang, C. Liu, C. Shen, Z. Guo, *ACS Appl. Mater. Interfaces* **2019**, *11*, 21904.
[37] A. V. Hoang-Phuong Phan, T. Dinh, T.-K. Nguyen, D. V. D. Abu Riduan Md Foisal, A. Qamar, A. R. Kermany, N.-T. Nguyen, *Appl. Phys. Lett.* **2019**, *110*, 144101.
[38] L. Lao, D. Shou, Y. S. Wu, J. T. Fan, *Sci. Adv.* **2020**, *6*, eaaz0013.
[39] X. Wang, Z. Huang, D. Miao, J. Zhao, J. Yu, B. Ding, *ACS Nano* **2018**, *13*, 1060.
[40] D. Shou, J. Fan, *Adv. Funct. Mater.* **2018**, *28*, 1800269.
[41] Y. Peng, W. Li, B. Liu, W. Jin, J. Schaadt, J. Tang, G. Zhou, G. Wang, J. Zhou, C. Zhang, Y. Zhu, W. Huang, T. Wu, K. E. Goodson, C. Dames, R. Prasher, S. Fan, Y. Cui, *Nat. Commun.* **2021**, *12*, 6122.
[42] M. W. Toepke, D. J. Beebe, *Lab Chip* **2006**, *6*, 1484.